

# Human Structural Homologues of SARS-CoV-2 PL<sup>pro</sup> as Anti-Targets: A Strategic Panel Analysis

Abdullah I. Al-Homoudi<sup>1</sup>, Joseph Engel<sup>1</sup>, Michael D. Muczynski<sup>1</sup>, Joseph S. Brunzelle<sup>2</sup>, Navnath S. Gavande<sup>3,4</sup>, Ladislau C. Kovari<sup>1§</sup>

<sup>1</sup>Dept. of Biochemistry, Microbiology and Immunology, Wayne State University, School of Medicine, Detroit, MI, USA

<sup>2</sup>Synchrotron Research Center, Life Science Collaborative Access Team, Northwestern University, Argonne, IL, USA

<sup>3</sup>Dept. of Pharmaceutical Sciences, Eugene Applebaum College of Pharmacy and Health Sciences, Wayne State University, Detroit, MI, USA

<sup>4</sup>Molecular Therapeutics Program, Barbara Ann Karmanos Cancer Institute, Wayne State University, School of Medicine, Detroit, MI, USA

§To whom correspondence should be addressed: kovari@med.wayne.edu

## Abstract

COVID-19 is caused by SARS-CoV-2, a highly transmissible and pathogenic RNA betacoronavirus. Developing small-molecule antiviral inhibitors of the SARS-CoV-2 papain-like protease (PL<sup>pro</sup>) is advantageous due to the enzyme's role in processing viral polyproteins and disrupting host immune sensing. Given the structural and functional similarities between PL<sup>pro</sup> and human deubiquitinases (DUBs), small-molecule inhibitors are frequently counter-screened for off-target activity using a panel of human DUBs. Through X-ray crystallography, DALI structural comparisons, and *in silico* analysis, a high-quality crystal structure of SARS-CoV-2 PL<sup>pro</sup> enabled the identification of the closest structural human homologues of PL<sup>pro</sup>. Among the 27 human DUBs identified, USP46 and USP12 displayed the greatest structural similarity to PL<sup>pro</sup>, with alignment scores below 0.45 and RMSD values of 3.0 Å or less. Additionally, binding sites on ubiquitin-specific protease (USP46) and USP12, ancillary to the active site residues, share high sequence identity to the PL<sup>pro</sup> substrate binding sites that are often engaged by the most potent PL<sup>pro</sup> inhibitors. These findings offer a strong basis for choosing anti-targets and serve as a foundation for designing selective small-molecule PL<sup>pro</sup> inhibitors.

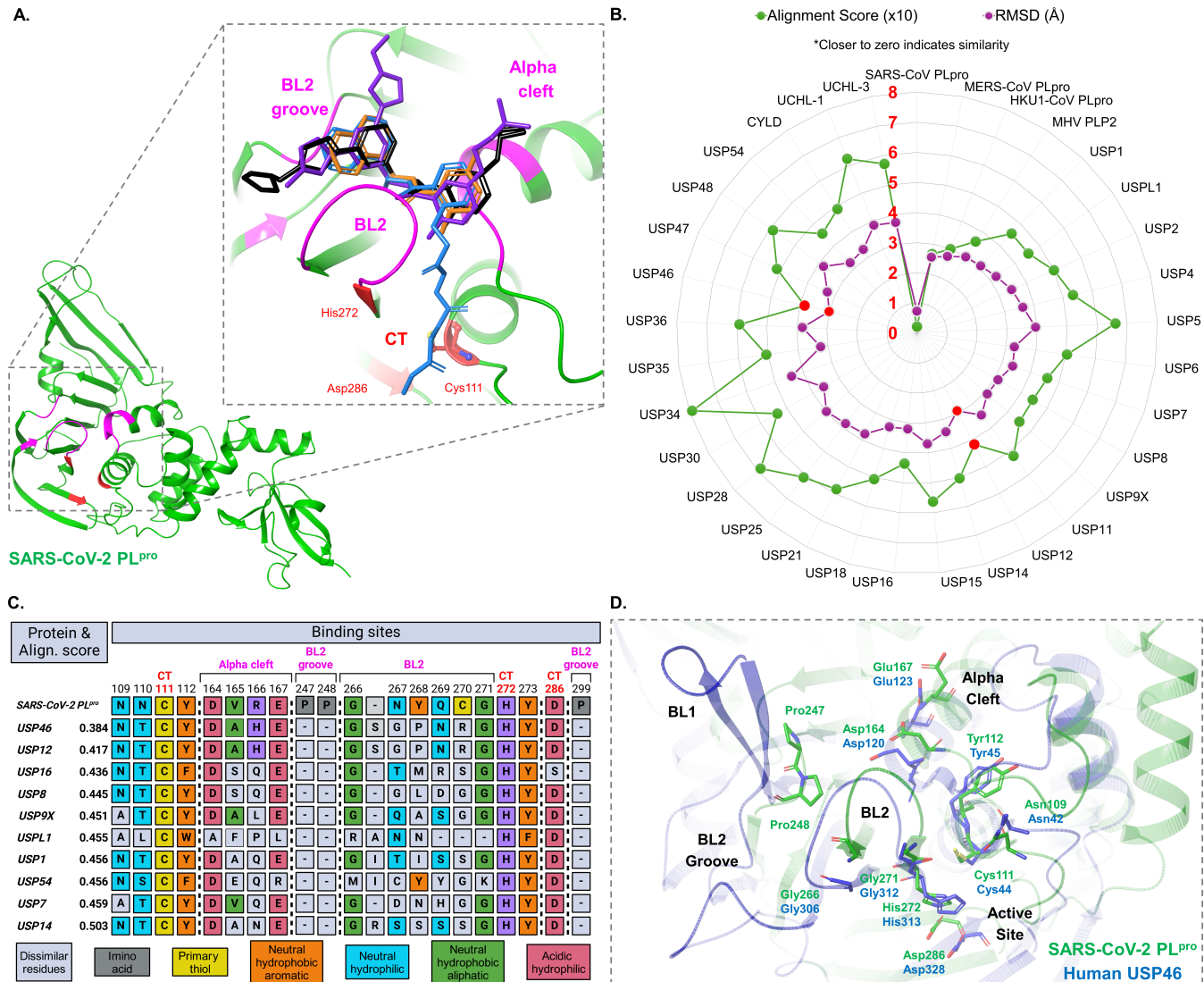


**Figure 1. Identifying the closest structural human homologues of SARS-CoV-2 PL<sup>pro</sup>:**

(A) The structure of SARS-CoV-2 PL<sup>pro</sup> (9BF8.pdb) is represented by a green, pink, and red ribbon, alongside the binding poses of the most potent small-molecule inhibitors of SARS-CoV-2 PL<sup>pro</sup>. The inhibitors (thick tube representations) include GRL-0617 (orange, 7CJM.pdb), Compound 7 (blue, 8EUA.pdb), XR8-24 (black, 7LBS.pdb), and Jun12682 (purple, 8UOB.pdb), which interact with binding sites (pink) that are ancillary to active site residues Cys111, His272, and Asp286 (red). The relevant binding sites are known as the blocking loop (BL2) (Gly266-Gly-271), BL2 groove (Pro247, Pro248, Pro299, Gly266), and the Alpha-cleft (Asp164-Glu167) binding sites (pink). (B) Radar plot illustrating structural alignment results of related coronavirus (CoV) PL<sup>pro</sup> from SARS-CoV, MERS-CoV, HKU1-CoV, murine hepatitis virus (MHV), and the catalytic domains of 27 human deubiquitinases (DUBs). Alignment scores (green) lower than 0.6 indicate a good alignment, while scores greater than 0.6 indicate a failure of structural alignment calculation and insufficient structural similarity for a meaningful alignment. RMSD (Å) (purple) is the distance between superpositioned atoms, calculated based only on the residues that have been successfully aligned. The plot highlights the closest human structural homologues of SARS-CoV-2 PL<sup>pro</sup>, which are ubiquitin-specific protease 46 (USP46) and USP12 (red data blocks). (C) Binding site amino acid sequence alignment and Alignment scores of unrelated human structural protease homologues of SARS-CoV-2 PL<sup>pro</sup> (Created in BioRender. Alhomoudi, A. (2025) <https://BioRender.com/gpsv9cp>). (D) The figure illustrates the structural superposition of binding sites for USP46 (blue, 5L8H.pdb) and SARS-CoV-2 PL<sup>pro</sup> (green, 9BF8.pdb), emphasizing the BL2 groove, Alpha-cleft, and BL1, a secondary blocking loop present on USP46 in place of the BL2 groove.

## Description

Despite the global availability of SARS-CoV-2 protease inhibitor regimens, there remains a critical need to enhance their pharmacological properties, particularly in terms of oral bioavailability, metabolic stability, and specificity (Eng et al., 2022; Jiang et al., 2023; Shimizu et al., 2023). The Papain-like protease (PL<sup>PRO</sup>) is essential for the replication of human coronaviruses (hCoVs) as it processes polyproteins translated from viral RNA into functional nonstructural proteins (NSPs). In addition to processing viral polyproteins, hCoV PL<sup>PRO</sup> directly facilitates the evasion of host immune responses by cleaving ubiquitin and the ubiquitin-like interferon-stimulated gene 15 (ISG-15) from host protein conjugates (Thiel et al., 2003; Barretto et al., 2005; Linder et al., 2007; Linder et al., 2005; Shin et al., 2020). Therefore, inhibiting PL<sup>PRO</sup> offers a promising approach to reducing viral replication and boosting antiviral immunity.

Deubiquitination and deISGylation are essential regulatory mechanisms in many biological processes, including NF- $\kappa$ B signaling following host innate immune system activation during viral infection (Hochstrasser, 2000; Song & Li, 2021). Seven human Deubiquitinase (DUB) subfamilies function to cleave ubiquitin and ubiquitin-like adducts from substrate proteins (Balakirev et al., 2003; Burnett et al., 2003; Evans et al., 2003; Gan-Erdene et al., 2003; Verma et al., 2002; Wilkinson, 1997; Yeh et al., 2000). The ubiquitin-specific protease (USP) subfamily has raised particular interest due to its presence in different eukaryotic organisms and the varied functions ascribed to this subfamily of diverse proteases in normal and pathological conditions (Quesada et al., 2004). In 2005, around the same time that Quesada and colleagues identified 22 novel human USPs, the first crystal structure of the SARS-CoV PL<sup>PRO</sup> was elucidated (2FE8.pdb) (Ratia et al., 2006). Structural similarity screening through the entire Protein Data Bank (PDB) identified two significant human structural homologues of SARS-CoV PL<sup>PRO</sup>: USP14 and HAUSP7 (USP7) (Ratia et al., 2006). Since then, tens of thousands of crystal structures have been deposited into the PDB, and the emergence of the deadly MERS-CoV in 2012 and SARS-CoV-2 in 2019 has accelerated the structure-based drug design (SBDD) of protease inhibitors.

The outbreak of SARS-CoV in 2002 facilitated the development of the naphthyl methyl amine core from GRL-0617 as an inhibitor for PL<sup>PRO</sup> (Ghosh et al., 2009). Since then, GRL-0617 has been repurposed against SARS-CoV-2 PL<sup>PRO</sup>, and several potent analogs have been optimized using SBDD, including Compound 19, Compound 7, XR8-24, and Jun12682 (Ratia et al., 2008; Sanders et al., 2023; Shan et al., 2021; Tan et al., 2023) (**Fig. 1A**). These potent antiviral compounds (Enzymatic IC<sub>50</sub>  $\geq$  0.09  $\mu$ M, Antiviral EC<sub>50</sub>  $\geq$  0.42  $\mu$ M) exhibit comparable binding poses, interacting with residues involved in ubiquitin and ISG-15 recognition, as evidenced by various hCoV PL<sup>PRO</sup> X-ray co-crystal structures with ubiquitin (4MM3.pdb, 4RF1.pdb, 6XAA.pdb) and ISG-15 (6XA9.pdb, 6BI8.pdb, 5TL6.pdb). Notably, the flexible “blocking loop” (BL2) (Gly266-Gly271), the hydrophobic BL2 groove (Pro247, Pro248, Pro299, Gly266), and the rigidifying Alpha cleft (Asp164-Glu167) of PL<sup>PRO</sup>, which are ancillary to the catalytic triad (Cys111, His272 & Asp286), improve inhibitor potency upon engagement. Although the efficacy of these compounds has been confirmed, the primary focus is now on enhancing pharmacological and drug-like attributes, including specificity and off-target activity.

Currently, the rationale for selecting specific USP panels for *in vitro* analysis to evaluate the specificity of PL<sup>PRO</sup> inhibitors and their off-target activity remains unclear. In the development of GRL-0617, Ratia et al. counter-screened against USP7, USP18, UCH-L1, and UCH-L3 (Ratia et al., 2008). In the development of Compound 19, Shan et al. counter-screened against USP36, USP14, USP8, USP7, USP2, and related DUBs UCH-L1, SNEP1, OTUB-1, ATAXIN3, and AMSH (Shan et al., 2021). Sanders et al. screened Compound 7 against USP2c, USP4, USP7, USP8, USP15, USP30, and UCH-L1 (Sanders et al., 2023). Lastly, XR8-24 and Jun12682 were counter-screened against only USP7 and USP14 (Tan et al., 2023). SBDD efforts would greatly benefit from a clearly defined panel of human DUBs, facilitating a more rational counter-screening of lead PL<sup>PRO</sup> inhibitors. To systematically address this concern, we identified a panel of the closest structural human homologues of SARS-CoV-2 PL<sup>PRO</sup> to counter-screen potential drug candidates

We crystallized the SARS-CoV-2 PL<sup>PRO</sup> enzyme (9BF8.pdb), and this high-quality crystal structure served as the query structure. The **9BF8 PDB Validation Report** contains relevant data collection and refinement statistics. The diffraction data were collected by the Life Sciences Collaborative Access Team (LS-CAT) using the NSLS-II 17-1 AMX beamline at the Brookhaven National Laboratory, resulting in a 1.85 Å resolution data set. The resulting refined model had an overall B-factor of 34.1 Å<sup>2</sup>, allowing proper main and side chain modeling. The phased and refined structure resulted in a final  $R_{\text{work}}$  of 17.75% ( $R_{\text{free}} = 20.00\%$ ), with zero Ramachandran and sidechain outliers.

A heuristic search of the PDB was performed using the DALI server (ekhidna2.biocenter.helsinki.fi/dali) to compare the coordinates of the query protein structure with all protein chains deposited in the PDB. The catalytic domains of 27 USPs were identified to have significant DALI Z-scores, where a higher score indicates statistical significance in similarity. DALI Z-

scores for identified USPs ranged from 9.5 to 13.8, with most having similar scores (**Data Set Identifying Structural Homologues of SARS-CoV-2 PL<sup>PRO</sup>**). SARS-CoV-2 PL<sup>PRO</sup> sequence identity of the identified USPs ranged from 9% to 16%. Other hits include SARS-CoV PL<sup>PRO</sup> and related hCoV PL<sup>PRO</sup> from MERS-CoV, hCoV-HKU1, and the murine hepatitis virus (MHV), which had Z-scores ranging from 32 to 44 and SARS-CoV-2 PL<sup>PRO</sup> sequence identities ranging from 28–83%.

Unlike the DALI server analysis, alignment metrics, such as the Alignment score in Schrödinger Maestro Suite release 2024-2 (version 14.0.134), provide a more comprehensive evaluation, offering a detailed and holistic view of protein similarity based on sequence and structure. In combination with the 27 USP catalytic cores identified by DALI, MERS-CoV PL<sup>PRO</sup>, hCoV-HKU1 PLP2, and Murine Hepatitis Virus (MHV) PLP2 were processed using the Maestro Protein Preparation Workflow to prepare structures, primarily to fill in missing side chains, and then subjected to the Protein Structure Alignment tool (Sastry et al., 2013). As expected, related CoV PL<sup>PRO</sup> had the best alignment scores to SARS-CoV-2 PL<sup>PRO</sup>, ranging from 0.021 to 0.3, respectively (**Fig. 1B**). The catalytic domains of USP46 and USP12 exhibited the highest structural homology with SARS-CoV-2 PL<sup>PRO</sup>, with alignment scores below 0.6 and RMSD values of  $\sim 3$  Å. The alignment scores of USP46 (0.368) and USP12 (0.384) were similar to the alignment score of the MHV PL<sup>PRO</sup> (0.361), highlighting the high similarity between the viral and human proteases (**Fig. 1C**). The catalytic domains of USP16, USP8, USP9X, USPL1, USP1, USP54, and USP7 are also significantly close structural homologues of PL<sup>PRO</sup> with alignment scores of less than 0.459 and RMSD of less than 3.37 Å. Nonetheless, USP16 lacks essential catalytic residues and is categorized as a non-protease homologue in accordance with the MEROPS database classification (**Fig. 1C**). This designation rules USP16 out as a viable PL<sup>PRO</sup> off-target. Furthermore, USPL1 and USP54 exhibit low PL<sup>PRO</sup> sequence identity in the BL2 and Alpha-cleft regions. Lastly, USP7's active site requires ubiquitin substrate binding for the catalytic Cys to align into an active conformation, and its BL2 is in an open state when HAUSP is unbound to ubiquitin (Hu et al., 2002), rendering it an irrational anti-PL<sup>PRO</sup> off-target. Overall, USP46, USP12, and USP9X are the closest human structural homologues to PL<sup>PRO</sup> (**Superposition of USP46, USP12, and USP9X to SARS-CoV-2 PL<sup>PRO</sup>**) and serve as the most rational off-targets for testing the specificity of small-molecule PL<sup>PRO</sup> inhibitors. Specifically, USP46 is notable for its superior alignment score, low RMSD value, and high sequence/structural identity with the ancillary binding sites of PL<sup>PRO</sup> (e.g., BL2) (**Fig. 1D**).

The methodology described can identify anti-target panels for developing antiviral compounds. The findings presented herein provide a more transparent and economical array of human proteins suitable for counter-screening compounds. This advancement consequently facilitates the development of potent and selective antiviral small-molecule PL<sup>PRO</sup> inhibitors.

## Methods

### PL<sup>PRO</sup> Cloning, Expression, and Purification

The gene encoding the full-length SARS-CoV-2 PL<sup>PRO</sup> (isolate Wuhan-Hu-1 NC\_045512.2, pp1ab aa 1564–1878) with N-terminal His<sub>6</sub>-SUMO-cleavable tag was cloned into pMCSG7 (Midwest Center for Structural Genomics) vector following the Ligation Independent Cloning (LIC) procedure (Stols et al., 2002). Whole Plasmid Sequencing was performed by Plasmidsaurus using Oxford Nanopore Technology with custom analysis and annotation. The pHis<sub>6</sub>-SUMO vector containing the PL<sup>PRO</sup> gene was transformed into Rosetta2 *E. coli* cells, plated onto Amp<sup>+</sup> agar plates, and incubated overnight at 37°C. Single colonies were cultured overnight in LB media with 100 µg/mL Amp at 37°C until OD<sub>600</sub> = 1.0. The temperature was then lowered to 20°C for 1 hour, followed by the induction of protein expression with 0.4 mM IPTG. The next day, cell pellets were harvested by centrifugation and frozen at -80°C. Frozen cell pellets were lysed by sonication in lysis buffer (25 mM Tris-HCl, pH 7.5, 150 mM NaCl, 1 mM DTT) containing 10 µg/mL lysozyme, 0.5 µg/mL Aprotinin, and 0.05 µg/mL Leupeptin. The lysate was clarified by centrifugation and loaded onto a 5 mL Ni-NTA resin equilibrated with Ni column wash buffer (25 mM Tris HCl, pH 7.5, 150 mM NaCl). Bound His<sub>6</sub>-SUMO-PL<sup>PRO</sup> was eluted with elution buffer (25 mM Tris-HCl, pH 7.5, 150 mM NaCl, and 300 mM imidazole). Fractions containing His<sub>6</sub>-SUMO-PL<sup>PRO</sup> were pooled and exchanged into SUMO dialysis buffer (20 mM Tris-HCl, pH 7.5, 250 mM NaCl, 1 mM DTT). A 1:100 molar ratio of ULPL1 (SUMO-specific protease) to PL<sup>PRO</sup> was incubated at 4°C overnight to cleave the His<sub>6</sub>-tag. The reaction was loaded onto a Ni-NTA resin re-equilibrated with 25 mM Tris-HCl, pH 7.5, and 150 mM NaCl to remove the tag and the SUMO-specific protease. Cleaved PL<sup>PRO</sup> eluted first, followed by gel filtration. PL<sup>PRO</sup> fractions were pooled, concentrated, and frozen in liquid nitrogen for storage at -80°C in S75 buffer (20 mM Tris-HCl, pH 7.5, 250 mM NaCl, 1 mM DTT). A Bradford assay using BSA as a standard monitored protein yield at each step.

### Crystallization and structure determination of SARS-CoV-2 PL<sup>PRO</sup>

The crystals of SARS-CoV-2 PL<sup>pro</sup> were grown using the sitting drop vapor diffusion method against a 300 µL reservoir solution at 4°C. The PL<sup>pro</sup> crystals were formed by mixing 1-2 µL of 18.7 mg/mL protein with 1 µL of reservoir solution containing 0.1 M Tris buffer (pH 7.0), 1 M sodium phosphate monobasic monohydrate (NaH<sub>2</sub>PO<sub>4</sub>), 1 M potassium phosphate dibasic (K<sub>2</sub>HPO<sub>4</sub>), and 3% w/v sucrose. Crystals formed over 1-2 days, reaching dimensions of 0.5-0.8 mm with octahedral and dodecahedral external symmetries. Full-sized crystals were harvested after one week. They were carefully transferred into a cryoprotectant consisting of mother liquor and 25% (v/v) glycerol before being flash-frozen in liquid nitrogen. The samples were subsequently shipped to the NSLS-II 17-1 AMX beamline at Brookhaven National Laboratory for diffraction data collection. Reflections were integrated and scaled using XDS and AIMLESS via Xia2 (P. Evans, 2006; Kabsch, 2010; Winter, 2010). Phases were calculated through molecular replacement using PHASER within the PHENIX software package (Adams et al., 2010; Liebschner et al., 2019; McCoy et al., 2007) for molecular structure determination by employing a monomeric SARS-CoV-2 PL<sup>pro</sup> structure (8FWN.pdb) as the search model. Automated model building and multiple rounds of refinement were conducted using PHENIX Autobuild, WinCoot, and PHENIX Refine (Afonine et al., 2012; Afonine et al., 2018; Echols et al., 2012; Emsley, Lohkamp, Scott, & Cowtan, 2010; Terwilliger et al., 2008). The X-ray crystal structure of SARS-CoV-2 PL<sup>pro</sup> has been deposited in the PDB (9BF8.pdb), and the deposition validation file is also provided.

### Structure Similarity Analysis

The query crystal structure PDB coordinates (9BF8.pdb) were uploaded into the DALI protein structure comparison server to perform a heuristic PDB search. Identified structures were prepared and aligned using the Protein Preparation Workflow and Protein Structure Alignment tool, employing the query crystal structure as reference residues using Schrödinger Maestro Suite release 2024-2 (version 14.0.134).

### Reagents

Plasmid	Description
pHis <sub>6</sub> -SUMO-PL <sup>pro</sup>	Custom bacterial vector with an ampicillin resistance marker for regulated expression of SARS-CoV-2 PL <sup>pro</sup> with a cleavable His <sub>6</sub> -SUMO tag.

### [Proteopedia Molecular Tour](#)

**Acknowledgements:** This research used resources of the Advanced Photon Source, a U.S. Department of Energy (DOE) Office of Science User Facility operated for the DOE Office of Science by Argonne National Laboratory under Contract No. DE-AC02-06CH11357. Use of the LS-CAT Sector 21 was supported by the Michigan Economic Development Corporation and the Michigan Technology Tri-Corridor (Grant 085P1000817).

### Extended Data

Description: Table with DALI-Z and Schrödinger Maestro Suite metrics used for analysis. . Resource Type: Dataset. File: [Data Set Identifying Structural Homologues of SARS-CoV-2 PL<sub>pro</sub>.pdf](#). DOI: [10.22002/cq58r-x9918](#)

Description: Full wwPDB X-ray structure validation report and statistics for PDB code 9BF8 SARS-CoV-2 PL<sub>pro</sub> Untagged Crystal Structure.. Resource Type: Collection. File: [9BF8 PDB Validation Report.pdf](#). DOI: [10.22002/ncxnv-byp09](#)

Description: Structural superposition of USP46, USP12, and USP9X to SARS-CoV-2 PL<sub>pro</sub> highlighting relevant binding sites.. Resource Type: Image. File: [Superposition of USP46, USP12, and USP9X to SARS-CoV-2 PL<sub>pro</sub>.pdf](#). DOI: [10.22002/7dxa1-p2863](#)

### References

Adams PD, Afonine PV, Bunkóczi Gb, Chen VB, Davis IW, Echols N, et al., Zwart. 2010. *PHENIX*: a comprehensive Python-based system for macromolecular structure solution. Acta Crystallographica Section D Biological Crystallography 66: 213-221. DOI: [10.1107/s0907444909052925](#)

Afonine PV, Grosse-Kunstleve RW, Echols N, Headd JJ, Moriarty NW, Mustyakimov M, et al., Adams. 2012. Towards automated crystallographic structure refinement with *phenix.refine*. Acta Crystallographica Section D Biological Crystallography 68: 352-367. DOI: [10.1107/s0907444912001308](#)

- Afonine PV, Poon BK, Read RJ, Sobolev OV, Terwilliger TC, Urzhumtsev A, Adams PD. 2018. Real-space refinement in*PHENIX* for cryo-EM and crystallography. *Acta Crystallographica Section D Structural Biology* 74: 531-544. DOI: [10.1107/s2059798318006551](https://doi.org/10.1107/s2059798318006551)
- Balakirev MY, Tcherniuk SO, Jaquinod M, Chroboczek J. 2003. Otubains: a new family of cysteine proteases in the ubiquitin pathway. *EMBO reports* 4: 517-522. DOI: [10.1038/sj.embor.embor824](https://doi.org/10.1038/sj.embor.embor824)
- Barretto N, Jukneliene D, Ratia K, Chen Z, Mesecar AD, Baker SC. 2005. The papain-like protease of severe acute respiratory syndrome coronavirus has deubiquitinating activity. *J Virol* 79(24): 15189-98. PubMed ID: [16306590](https://pubmed.ncbi.nlm.nih.gov/16306590/)
- Burnett B. 2003. The polyglutamine neurodegenerative protein ataxin-3 binds polyubiquitylated proteins and has ubiquitin protease activity. *Human Molecular Genetics* 12: 3195-3205. DOI: [10.1093/hmg/ddg344](https://doi.org/10.1093/hmg/ddg344)
- Echols N, Grosse-Kunstleve RW, Afonine PV, Bunkóczi Gb, Chen VB, Headd JJ, et al., Adams. 2012. Graphical tools for macromolecular crystallography in*PHENIX*. *Journal of Applied Crystallography* 45: 581-586. DOI: [10.1107/S0021889812017293](https://doi.org/10.1107/S0021889812017293)
- Emsley P, Lohkamp B, Scott WG, Cowtan K. 2010. Features and development of *Coot*. *Acta Crystallographica Section D Biological Crystallography* 66: 486-501. DOI: [10.1107/s0907444910007493](https://doi.org/10.1107/s0907444910007493)
- Eng H, Dantonio AL, Kadar EP, Obach RS, Di L, Lin J, et al., Kalgutkar. 2022. Disposition of Nirmatrelvir, an Orally Bioavailable Inhibitor of SARS-CoV-2 3C-Like Protease, across Animals and Humans. *Drug Metabolism and Disposition* 50: 576-590. DOI: [10.1124/dmd.121.000801](https://doi.org/10.1124/dmd.121.000801)
- Evans P. 2005. Scaling and assessment of data quality. *Acta Crystallographica Section D Biological Crystallography* 62: 72-82. DOI: [10.1107/s0907444905036693](https://doi.org/10.1107/s0907444905036693)
- Evans PC, Smith TS, Lai MJ, Williams MG, Burke DF, Heyninck K, et al., Kilshaw. 2003. A Novel Type of Deubiquitinating Enzyme. *Journal of Biological Chemistry* 278: 23180-23186. DOI: [10.1074/jbc.M301863200](https://doi.org/10.1074/jbc.M301863200)
- Gan-Erdene T, Nagamalleswari K, Yin L, Wu K, Pan ZQ, Wilkinson KD. 2003. Identification and Characterization of DEN1, a Deneddylase of the ULP Family. *Journal of Biological Chemistry* 278: 28892-28900. DOI: [10.1074/jbc.M302890200](https://doi.org/10.1074/jbc.M302890200)
- Ghosh AK, Takayama J, Aubin Y, Ratia K, Chaudhuri R, Baez Y, et al., Mesecar. 2009. Structure-Based Design, Synthesis, and Biological Evaluation of a Series of Novel and Reversible Inhibitors for the Severe Acute Respiratory Syndrome-Coronavirus Papain-Like Protease. *Journal of Medicinal Chemistry* 52: 5228-5240. DOI: [10.1021/jm900611t](https://doi.org/10.1021/jm900611t)
- Hochstrasser M. 2000. Evolution and function of ubiquitin-like protein-conjugation systems. *Nature Cell Biology* 2: E153-E157. DOI: [10.1038/35019643](https://doi.org/10.1038/35019643)
- Hu M, Li P, Li M, Li W, Yao T, Wu JW, et al., Shi. 2002. Crystal Structure of a UBP-Family Deubiquitinating Enzyme in Isolation and in Complex with Ubiquitin Aldehyde. *Cell* 111: 1041-1054. DOI: [10.1016/s0092-8674\(02\)01199-6](https://doi.org/10.1016/s0092-8674(02)01199-6)
- Jiang X, Su H, Shang W, Zhou F, Zhang Y, Zhao W, et al., Xu. 2023. Structure-based development and preclinical evaluation of the SARS-CoV-2 3C-like protease inhibitor simnoretvir. *Nature Communications* 14: 10.1038/s41467-023-42102-y. DOI: [10.1038/s41467-023-42102-y](https://doi.org/10.1038/s41467-023-42102-y)
- Kabsch W. 2010. *XDS*. *Acta Crystallographica Section D Biological Crystallography* 66: 125-132. DOI: [10.1107/s0907444909047337](https://doi.org/10.1107/s0907444909047337)
- Liebschner D, Afonine PV, Baker ML, Bunkóczi Gb, Chen VB, Croll TI, et al., Adams. 2019. Macromolecular structure determination using X-rays, neutrons and electrons: recent developments in *Phenix*. *Acta Crystallographica Section D Structural Biology* 75: 861-877. DOI: [10.1107/s2059798319011471](https://doi.org/10.1107/s2059798319011471)
- Lindner HA, Lytvyn V, Qi H, Lachance P, Ziomek E, Ménard R. 2007. Selectivity in ISG15 and ubiquitin recognition by the SARS coronavirus papain-like protease. *Arch Biochem Biophys* 466(1): 8-14. PubMed ID: [17692280](https://pubmed.ncbi.nlm.nih.gov/17692280/)
- Lindner HA, Fotouhi-Ardakani N, Lytvyn V, Lachance P, Sulea T, Ménard R. 2005. The papain-like protease from the severe acute respiratory syndrome coronavirus is a deubiquitinating enzyme. *J Virol* 79(24): 15199-208. PubMed ID: [16306591](https://pubmed.ncbi.nlm.nih.gov/16306591/)
- Madhavi Sastry G, Adzhigirey M, Day T, Annabhimoju R, Sherman W. 2013. Protein and ligand preparation: parameters, protocols, and influence on virtual screening enrichments. *Journal of Computer-Aided Molecular Design* 27: 221-234. DOI: [10.1007/s10822-013-9644-8](https://doi.org/10.1007/s10822-013-9644-8)
- McCoy AJ, Grosse-Kunstleve RW, Adams PD, Winn MD, Storoni LC, Read RJ. 2007. *Phaser* crystallographic software. *Journal of Applied Crystallography* 40: 658-674. DOI: [10.1107/s0021889807021206](https://doi.org/10.1107/s0021889807021206)

Quesada Vc, Díaz-Perales A, Gutiérrez-Fernández A, Garabaya C, Cal S, López-Otín C. 2004. Cloning and enzymatic analysis of 22 novel human ubiquitin-specific proteases. *Biochemical and Biophysical Research Communications* 314: 54-62. DOI: [10.1016/j.bbrc.2003.12.050](https://doi.org/10.1016/j.bbrc.2003.12.050)

Ratia K, Pegan S, Takayama J, Sleeman K, Coughlin M, Baliji S, et al., Mesecar. 2008. A noncovalent class of papain-like protease/deubiquitinase inhibitors blocks SARS virus replication. *Proceedings of the National Academy of Sciences* 105: 16119-16124. DOI: [doi:10.1073/pnas.0805240105](https://doi.org/10.1073/pnas.0805240105)

Ratia K, Saikatendu KS, Santarsiero BD, Barretto N, Baker SC, Stevens RC, Mesecar AD. 2006. Severe acute respiratory syndrome coronavirus papain-like protease: Structure of a viral deubiquitinating enzyme. *Proceedings of the National Academy of Sciences* 103: 5717-5722. DOI: [doi:10.1073/pnas.0510851103](https://doi.org/10.1073/pnas.0510851103)

Sanders BC, Pokhrel S, Labbe AD, Mathews II, Cooper CJ, Davidson RB, et al., Parks. 2023. Potent and selective covalent inhibition of the papain-like protease from SARS-CoV-2. *Nature Communications* 14: 10.1038/s41467-023-37254-w. DOI: [10.1038/s41467-023-37254-w](https://doi.org/10.1038/s41467-023-37254-w)

Shan H, Liu J, Shen J, Dai J, Xu G, Lu K, et al., Tan. 2021. Development of potent and selective inhibitors targeting the papain-like protease of SARS-CoV-2. *Cell Chemical Biology* 28: 855-865.e9. DOI: [10.1016/j.chembiol.2021.04.020](https://doi.org/10.1016/j.chembiol.2021.04.020)

Shimizu R, Sonoyama T, Fukuhara T, Kuwata A, Matsuzaki T, Matsuo Y, Kubota R. 2023. Evaluation of the Drug-Drug Interaction Potential of Ensitrelvir Fumaric Acid with Cytochrome P450 3A Substrates in Healthy Japanese Adults. *Clinical Drug Investigation* 43: 335-346. DOI: [10.1007/s40261-023-01265-8](https://doi.org/10.1007/s40261-023-01265-8)

Shin D, Mukherjee R, Grewe D, Bojkova D, Baek K, Bhattacharya A, et al., Dikic. 2020. Papain-like protease regulates SARS-CoV-2 viral spread and innate immunity. *Nature* 587: 657-662. DOI: [10.1038/s41586-020-2601-5](https://doi.org/10.1038/s41586-020-2601-5)

Song K, Li S. 2021. The Role of Ubiquitination in NF- $\kappa$ B Signaling during Virus Infection. *Viruses* 13: 145. DOI: [doi.org/10.3390/v13020145](https://doi.org/10.3390/v13020145)

Stols L, Gu M, Dieckman L, Raffin R, Collart FR, Donnelly MI. 2002. A New Vector for High-Throughput, Ligation-Independent Cloning Encoding a Tobacco Etch Virus Protease Cleavage Site. *Protein Expression and Purification* 25: 8-15. DOI: [10.1006/prep.2001.1603](https://doi.org/10.1006/prep.2001.1603)

Tan B, Zhang X, Ansari A, Jadhav P, Tan H, Li K, et al., Wang. 2023. Design of SARS-CoV-2 papain-like protease inhibitor with antiviral efficacy in a mouse model. : 10.1101/2023.12.01.569653. DOI: [10.1101/2023.12.01.569653](https://doi.org/10.1101/2023.12.01.569653)

Terwilliger TC, Grosse-Kunstleve RW, Afonine PV, Moriarty NW, Zwart PH, Hung LW, Read RJ, Adams PD. 2007. Iterative model building, structure refinement and density modification with the *PHENIX AutoBuild*wizard. *Acta Crystallographica Section D Biological Crystallography* 64: 61-69. DOI: [10.1107/s090744490705024x](https://doi.org/10.1107/s090744490705024x)

Thiel V, Ivanov KA, Putics Á, Hertzog T, Schelle B, Bayer S, et al., Ziebuhr J. 2003. Mechanisms and enzymes involved in SARS coronavirus genome expression. *J Gen Virol* 84(Pt 9): 2305-2315. PubMed ID: [12917450](https://pubmed.ncbi.nlm.nih.gov/12917450/)

Verma R, Aravind L, Oania R, McDonald WH, Yates JR, Koonin EV, Deshaies RJ. 2002. Role of Rpn11 Metalloprotease in Deubiquitination and Degradation by the 26 S Proteasome. *Science* 298: 611-615. DOI: [doi:10.1126/science.1075898](https://doi.org/10.1126/science.1075898)

Wilkinson KD. 1997. Regulation of ubiquitin-dependent processes by deubiquitinating enzymes. *The FASEB Journal* 11: 1245-1256. DOI: [10.1096/fasebj.11.14.9409543](https://doi.org/10.1096/fasebj.11.14.9409543)

Winter G. 2009. *xia2*: an expert system for macromolecular crystallography data reduction. *Journal of Applied Crystallography* 43: 186-190. DOI: [doi:10.1107/S0021889809045701](https://doi.org/10.1107/S0021889809045701)

Yeh ETH, Gong L, Kamitani T. 2000. Ubiquitin-like proteins: new wines in new bottles. *Gene* 248: 1-14. DOI: [10.1016/s0378-1119\(00\)00139-6](https://doi.org/10.1016/s0378-1119(00)00139-6)

**Funding:** Partial support for this research is provided by NIH (grant AI161570).

**Author Contributions:** Abdullah I. Al-Homoudi: writing - original draft, conceptualization, data curation, visualization, investigation. Joseph Engel: writing - review editing. Michael D. Muczynski: writing - review editing. Joseph S. Brunzelle: data curation. Navnath S. Gavande: supervision. Ladislau C. Kovari: supervision.

**Reviewed By:** Anonymous

**History:** Received November 16, 2024 **Revision Received** March 29, 2025 **Accepted** March 17, 2025 **Published Online** April 14, 2025 **Indexed** April 28, 2025

---

4/14/2025 - Open Access

**Copyright:** © 2025 by the authors. This is an open-access article distributed under the terms of the Creative Commons Attribution 4.0 International (CC BY 4.0) License, which permits unrestricted use, distribution, and reproduction in any medium, provided the original author and source are credited.

**Citation:** Al-Homoudi AI, Engel J, Muczynski MD, Brunzelle JS, Gavande NS, Kovari LC. 2025. Human Structural Homologues of SARS-CoV-2 PL<sup>PRO</sup> as Anti-Targets: A Strategic Panel Analysis. microPublication Biology. [10.17912/micropub.biology.001418](https://doi.org/10.17912/micropub.biology.001418)